[4] Z. Ding, S. M. Perlaza, I. Esnaola, and H. V. Poor, "Power allocation strategies in energy harvesting wireless cooperative networks," *IEEE Trans. Wireless Commun.*, vol. 13, no. 2, pp. 846–860, Feb. 2014.
[5] I. Krikidis, "Simultaneous information and energy transfer in large-scale networks with/without relaying," *IEEE Trans. Commun.*, vol. 62, no. 3, pp. 900–912, Mar. 2014.
[6] Z. Ding, I. Krikidis, B. Sharif, and H. V. Poor, "Wireless information and power transfer in cooperative networks with spatially random relays," *IEEE Trans. Wireless Commun.*, vol. 13, no. 8, pp. 4440–4453, Aug. 2014.
[7] A. Minasian, S. ShahbazPanahi, and R. S. Adve, "Energy harvesting cooperative communication systems," *IEEE Trans. Wireless Commun.*, vol. 13, no. 11, pp. 6118–6131, Nov. 2014.
[8] C. Huang, R. Zhang, and S. Cui, "Throughput maximization for the Gaussian relay channel with energy harvesting constraints," *IEEE J. Sel. Areas Commun.*, vol. 31, no. 8, pp. 1469–1479, Aug. 2013.
[9] I. Ahmed, A. Ikhlef, R. Schober, and R. K. Mallik, "Joint power allocation and relay selection in energy harvesting AF relay systems," *IEEE Wireless Commun. Lett.*, vol. 2, no. 2, pp. 239–242, Apr. 2013.
[10] M. Peng, Y. Liu, D. Wei, W. Wang, and H.-H. Chen, "Hierarchical cooperative relay based heterogeneous networks," *IEEE Wireless Commun.*, vol. 18, no. 3, pp. 48–56, Jun. 2011.
[11] B. Zhou, H. Hu, S.-Q. Huang, and H.-H. Chen, "Intracluster device-to-device relay algorithm with optimal resource allocation," *IEEE Trans. Veh. Technol.*, vol. 62, no. 5, pp. 2315–2326, Jun. 2013.
[12] T. Le, K. Mayaram, and T. Fiez, "Efficient far-field radio frequency energy harvesting for passively powered sensor networks," *IEEE J. Solid-State Circuits*, vol. 43, no. 5, pp. 1287–1302, May 2008.
[13] F. Azmat, Y. Chen, and N. G. Stocks, "Predictive modelling of RF energy for wireless powered communications," *IEEE Commun. Lett.*, vol. 20, no. 1, pp. 173–176, Jan. 2016.
[14] I. S. Gradshteyn and I. M. Ryzhik, *Table of Integrals, Series, and Products*, 6th ed. New York, NY, USA: Academic, 2000.
[15] R. K. Ganti and M. Haenggi, "Spatial analysis of opportunistic downlink relaying in a two-hop cellular system," *IEEE Trans. Commun.*, vol. 60, no. 5, pp. 1443–1450, May 2012.
[16] F. H. Khan, Y. Chen, and M.-S. Alouini, "Novel receivers for AF relaying with distributed STBC using cascaded and disintegrated channel estimation," *IEEE Trans. Wireless Commun.*, vol. 11, no. 4, pp. 1370–1379, Apr. 2012.
[17] J. Chen *et al.*, "Dynamic channel assignment for wireless sensor networks," *IEEE Trans. Parallel Distrib. Syst.*, vol. 26, no. 1, pp. 95–106, Jan. 2015.
[18] J. Chen *et al.*, "Game theoretical approach for channel allocation in wireless sensor and actuator networks," *IEEE Trans. Autom. Control*, vol. 56, no. 10, pp. 2332–2344, Oct. 2011.
[19] Y. Zeng and R. Zhang, "Full-duplex wireless-powered relay with self-energy recycling," *IEEE Wireless Commun. Lett.*, vol. 4, no. 2, pp. 201–204, Apr. 2015.

Generalized-Spatial-Modulation-Based Reduced-RF-Chain Millimeter-Wave Communications

Naoki Ishikawa, *Student Member, IEEE*, Rakshith Rajashekar, *Member, IEEE*, Shinya Sugiura, *Senior Member, IEEE*, and Lajos Hanzo, *Fellow, IEEE*

***Abstract*—A generalized spatial modulation (GSM)-based millimeter-wave communications system is proposed. The GSM transmitter is characterized by a lower number of radio frequency (RF) chains than the number of transmit antennas; hence, it is capable of reducing both the transmitter cost and the energy consumption. The antenna array alignment is optimized so as to maximize the rank of the channel matrix encountered. Furthermore, we employ an array of analog beamformers, which allows us to benefit both from the beamforming gain and from the GSM scheme's high rate. It is demonstrated that the constrained capacity of the GSM transmitter equipped with as few as two RF chains is capable of approaching the performance of the full-RF spatial multiplexing having eight RF chains.**

***Index Terms*—Analog beamforming, channel capacity, constrained capacity, generalized spatial modulation (GSM), line-of-sight (LoS), millimeter-wave (mmWave), multiple-input multiple-output (MIMO), multiplexing.**

I. Introduction

Spatial modulation (SM)-aided multiple-input multiple-output (MIMO) schemes are capable of increasing the attainable data rate with the aid of a single radio frequency (RF) transmitter [1]. In the SM transmitter, the information bits are mapped to transmitted symbols by activating a single transmit antenna (TA) element out of multiple TA elements, and only a single symbol is transmitted from the activated TA. This allows us to avoid the interchannel interference at the receiver; hence, low-complexity single-stream decoding [2], [3] is applicable. Furthermore, the single-RF transmitter structure specific to the SM scheme reduces static power consumption [4]. In [5] and [6], the SM scheme was extended to a more flexible framework referred to as the generalized SM (GSM), where multiple antenna elements are simultaneously activated in each symbol duration. More specifically, the GSM scheme subsumes several classic MIMO schemes, such as the SM and Bell Laboratories Layered Space-Time (BLAST) schemes [7].

In millimeter-wave (mmWave) communications [8], the rank of the MIMO channel matrix tends to be low, due to the presence of a strong line-of-sight (LoS) component. In [9], the antenna alignment was specifically adjusted for increasing the rank of the channel matrix in an mmWave MIMO scenario. In [10] and [11], an antenna array architecture of multiple beamformers was employed, where each beamfomer

Manuscript received December 18, 2015; revised March 10, 2016; accepted April 14, 2016. Date of publication April 20, 2016; date of current version January 13, 2017. The work of N. Ishikawa was supported in part by the SCAT Fellowship and in part by the MEXT/JASSO Tobitate Fellowship of Japan. The work of S. Sugiura was supported by the Japan Society for the Promotion of Science KAKENHI under Grant 26709028. The work of L. Hanzo was supported by the European Research Council's Advanced Fellow Grant Beam-Me-Up. The review of this paper was coordinated by Prof. Y. L. Guan.

N. Ishikawa and S. Sugiura are with the Department of Computer and Information Sciences, Tokyo University of Agriculture and Technology, Tokyo 184-8588, Japan (e-mail: naoki@ishikawa.cc; sugiura@ieee.org).

R. Rajashekar and L. Hanzo are with the School of Electronics and Computer Science, University of Southampton, Southampton SO17 1BJ, U.K. (e-mail: R.Mysore-Rajashekar@soton.ac.uk; lh@ecs.soton.ac.uk).

Color versions of one or more of the figures in this paper are available online at http://ieeexplore.ieee.org.

Digital Object Identifier 10.1109/TVT.2016.2555378

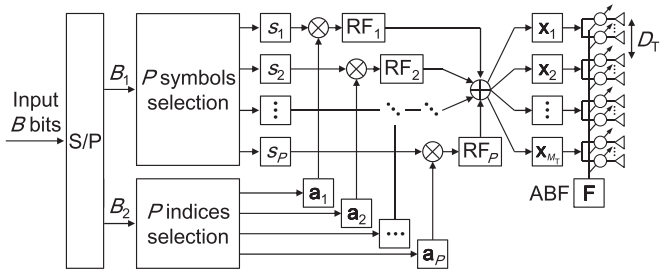

Fig. 1. Transmitter structure of our GSM scheme using an ABF array.

is spaced sufficiently apart from each other to experience independent fading. In [12], the antenna alignment scheme [9] was applied to a space-shift-keying-based mmWave system.

The detrimental effects of the high propagation loss in mmWave communications are particularly severe in an urban scenario [8]. To combat this limitation, it is beneficial to invoke beamforming at the transmitter and/or the receiver [10], [11], which operates with the aid of a high number of antenna elements. However, it may be disadvantageous to employ a full-digital beamforming-array architecture that has the same number of RF chains as that of the antenna elements, due to their high cost and high energy consumption. Recently, a hybrid beamforming arrangement, relying on both analog and digital beamformers, has been proposed in [13] and [14]. Here, a high number of antenna elements are divided into beamforming subarrays, where each beamformer is connected to an RF chain. Note that in the classic spatial-multiplexing MIMO system, the number of RF chains has to be equal to the number of multiplexed substreams.

Against this backcloth, the novel contribution of this letter is that we provide the design guideline for the reduced-RF-chain GSM-based mmWave architecture. More specifically, to benefit from both a beamforming gain and the GSM scheme's high rate, we employ an array of analog beamformers (ABFs), each consisting of multiple TA elements weighted by analog phase shifters. Furthermore, we optimized the spacing between the ABFs, so that the rank of the associated channel matrix is maximized. We demonstrate that the proposed GSM scheme using the beamfomer array is capable of reducing the number of RF chains at the transmitter, while maintaining high capacity, which is close to that of the conventional spatial-multiplexing scheme.[1]

II. System Model

A. Reduced-RF GSM Transmitter

Fig. 1 shows the schematic of our GSM transmitter, having N_T TA elements, which are partitioned into $M_{\rm T}$ ABFs, each consisting of $U_T = N_T/M_T$ TA elements and the same number of analog phase shifters. In our GSM transmitter, the number of RF chains P is less than the number of ABFs M_T, whereas the conventional spatial-multiplexing scheme requires a full-RF structure having $P = M_T$.

At the GSM transmitter, B information bits are mapped into a symbol vector $\mathbf{x} \in \mathbb{C}^{M_T \times 1}$ as follows. The B input bits are serial-to-parallel converted into $B_1 = P\log_2(\mathcal{L})$ bits and $B_2 = \lfloor \log_2 \binom{M_T}{P} \rfloor$ bits. The B_1 bits are modulated to P complex-valued symbols s_p $(p = 1, \ldots, P)$ with the aid of the classic quadrature amplitude modulation (QAM) or phase-shift keying (PSK) scheme, where the constellation size is given by $\mathcal{L}$. Based on the B_2 bits, P out of M_T ABFs are activated, where P index vectors $\mathbf{a}_p \in \mathbb{C}^{M_T \times 1}$ $(p = 1, \ldots, P)$ are selected out of the M_T legitimate vectors of $([1\ 0\ \cdots\ 0]^{\rm T}, [0\ 1\ \cdots\ 0]^{\rm T}, \ldots, [0\ 0\ \cdots\ 1]^{\rm T})$. Finally, the GSM transmitter generates a symbol vector $\mathbf{x}$ according to

$$\mathbf{x} = \frac{1}{\sqrt{P}} \sum_{p=1}^{P} s_p \mathbf{a}_p \tag{1}$$

which satisfies the average power constraint of $E[\|\mathbf{x}\|^2] = 1$, where $E[\bullet]$ represents the expectation operation. In advance of transmissions, the symbol vector $\mathbf{x}$ is precoded by a matrix $\mathbf{F} = \mathrm{diag}(\mathbf{f}_1, \ldots, \mathbf{f}_{M_T}) \in \mathbb{C}^{N_T \times M_T}$ [10], [11], where $\mathrm{diag}(\bullet)$ represents the block diagonalization, and $\mathbf{f}_i \in \mathbb{C}^{U_T \times 1}$ $(1 \le i \le M_T)$ represents the weight vectors of the ith ABF at the transmitter, which has the constraint of $\|\mathbf{f}_i\|^2 = 1$.

To further elaborate, in Table I, we exemplify the GSM symbol sets for the $(M_T, P) = (4, 2)$ and (8, 2) scenarios. Furthermore, note that the classic spatial multiplexing is a special case of the GSM scheme, where the number of RF chains P is equal to the number of ABFs M_T. Similarly, the conventional single-stream symbol transmission is also subsumed by the GSM framework, where we have $P = 1$ and $\mathbf{a}_1 = [1\ 1\ \cdots\ 1]^{\rm T}/\sqrt{M_T}$.

TABLE I
Example of the GSM Symbols for $(M_T, P) = (4,2)$ and (8,2)

$M_{\rm T}$	P	$\sqrt{P}\mathbf{x}$
4	2	$[s_1\ s_2\ 0\ 0]^{\rm T}$, $[s_1\ 0\ s_2\ 0]^{\rm T}$, $[0\ s_1\ 0\ s_2]^{\rm T}$, $[0\ 0\ s_1\ s_2]^{\rm T}$.
8	2	$[s_1\ 0\ 0\ s_2\ 0\ 0\ 0\ 0]^{\rm T}$, $[0\ 0\ s_1\ s_2\ 0\ 0\ 0\ 0]^{\rm T}$, $[s_1\ 0\ 0\ 0\ s_2\ 0\ 0\ 0]^{\rm T}$, $[0\ 0\ s_1\ 0\ 0\ s_2\ 0\ 0]^{\rm T}$, $[s_1\ 0\ 0\ 0\ 0\ s_2\ 0\ 0]^{\rm T}$, $[0\ 0\ 0\ s_1\ 0\ 0\ 0\ s_2]^{\rm T}$, $[s_1\ 0\ 0\ 0\ 0\ 0\ s_2\ 0]^{\rm T}$, $[0\ 0\ 0\ s_1\ 0\ s_2\ 0\ 0]^{\rm T}$, $[0\ s_1\ s_2\ 0\ 0\ 0\ 0\ 0]^{\rm T}$, $[0\ 0\ 0\ 0\ s_1\ 0\ s_2\ 0]^{\rm T}$, $[0\ s_1\ 0\ s_2\ 0\ 0\ 0\ 0]^{\rm T}$, $[0\ 0\ 0\ 0\ s_1\ 0\ 0\ s_2]^{\rm T}$, $[0\ s_1\ 0\ 0\ s_2\ 0\ 0\ 0]^{\rm T}$, $[0\ 0\ 0\ 0\ 0\ s_1\ 0\ s_2]^{\rm T}$, $[0\ s_1\ 0\ 0\ 0\ 0\ s_2\ 0]^{\rm T}$, $[0\ 0\ 0\ 0\ 0\ 0\ s_1\ s_2]^{\rm T}$.

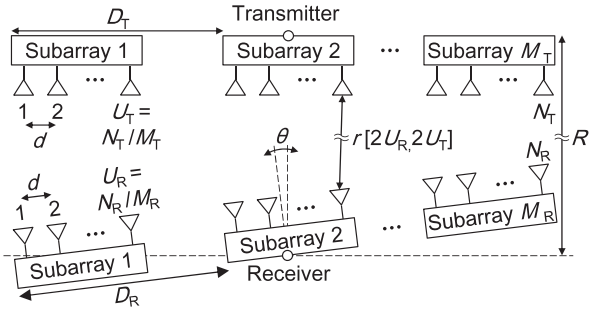

Fig. 2. ABF-array arrrangement of our GSM transmitter and receiver. The transmitter is located at a height of R, and the receiver is tilted at an angle of θ.

B. Channel Model

In this paper, we focus our attention on indoor mmWave communications, where a LoS component has the dominant effect [10]–[12], [16], [17] in comparison to the non-LoS paths. More specifically, we employ the frequency-flat Rician channel model. Fig. 2 shows the alignment of the ABF-array transmitter and receiver. The spacing between the ABF arrays at the transmitter and the receiver is represented by D_T and D_R, respectively. Moreover, d is the element separation of each antenna element. The transmitter is located at a height of R. The receiver has N_R antennas, and it is tilted at an angle of θ.

[1]Note that in mmWave communications, the bandwidth expansion caused by the SM-specific antenna switching [15] may not be a major problem, because a wide bandwidth is available.

The Rician fading channels are given by [9], [10], [12]

$$\mathbf{H} = \sqrt{\frac{K}{K+1}}\mathbf{H}_{\mathrm{LoS}} + \sqrt{\frac{1}{K+1}}\mathbf{H}_{\mathrm{NLoS}} \in \mathbb{C}^{N_R \times N_T} \quad (2)$$

where K is the Rice factor. Note that for the 60-GHz indoor communications scenario, the Rice factor K is in the range spanning from 8.34 to 12.04 dB [16]. Here, let us define the nth row and the mth column of $\mathbf{H}_{\mathrm{LoS}}$ by $\mathbf{H}_{\mathrm{LoS}}[n,m] = \exp(-j \cdot (2\pi/\lambda) \cdot r[n,m])$, where $r[n,m]$ is the distance between the mth TA and the nth receive antenna, whereas λ represents the wavelength. Furthermore, the nth row and the mth column of $\mathbf{H}_{\mathrm{NLoS}}$ obeys the zero-mean complex-valued Gaussian distribution, having a unit variance.

C. Receiver

Similar to the transmitter, the receiver consists of M_R ABFs, each having $U_R = N_R/M_R$ antenna elements. The receiver is equipped with the same number of RF chains as that of the ABFs, hence having a full-RF structure of $P = M_R$. The signals received at the M_R ABFs are given by

$$\mathbf{y} = \underbrace{\mathbf{W}^{\mathrm{H}}\mathbf{H}\mathbf{F}}_{\mathbf{H}_b}\mathbf{x} + \mathbf{n} \in \mathbb{C}^{M_R} \quad (3)$$

where $\mathbf{W} = \mathrm{diag}(\mathbf{w}_1, \ldots, \mathbf{w}_{M_R}) \in \mathbb{C}^{N_R \times M_R}$ [10], [11] is the ABF weight matrix associated with the analog phase shifters at the receiver, which satisfies the constraint of $\|\mathbf{w}_k\|^2 = 1 (1 \le k \le M_R)$. Furthermore, $\mathbf{n} \in \mathbb{C}^{M_R \times 1}$ denotes the additive white Gaussian noise having the variance of N_0, whereas $\mathbf{W}^{\mathrm{H}}\mathbf{H}\mathbf{F}$ is represented by the equivalent channel matrix $\mathbf{H}_b \in \mathbb{C}^{M_R \times M_T}$. In this paper, we assume that the receiver acquires accurate channels $\mathbf{H}_b$ with the aid of pilot symbols transmitted from the transmitter. Furthermore, the direction between the transmitter and the receiver is also known, which is used to determine the ABF weights $\mathbf{F}$ and $\mathbf{W}$ at the transmitter and the receiver, as will be shown in Section III-D.

Finally, the receiver estimates the transmitted information bits (B_1, B_2), based on the maximum-likelihood criterion as follows:

$$(\hat{B}_1, \hat{B}_2) = \arg \min_{(B_1, B_2)} \|\mathbf{y} - \mathbf{H}_b\mathbf{x}\|^2. \quad (4)$$

The reduced-complexity detection algorithms [2], [3], [18] developed for the GSM are readily applicable to the proposed receiver.

III. Channel Capacity

Here, we review the continuous-input–continuous-output memoryless channel (CCMC) capacity and the discrete-input–continuous-output memoryless channel (DCMC) capacity for our mmWave GSM scheme. The CCMC capacity is derived by assuming that the input signal obeys the Gaussian distribution, whereas in the derivation of the DCMC capacity, a specific finite-alphabet input symbol set is assumed.

A. CCMC Capacity

The classic CCMC capacity C_{CCMC} is given by [10], [14]

$$C_{\mathrm{CCMC}} = E_{\mathbf{H}}\left[\sum_{i=1}^{\mathrm{rank}(\mathbf{Q})} \log_2(1 + \mu_i\rho)\right] \text{ [bits/symbol]} \quad (5)$$

where we have

$$\mathbf{Q} = \begin{cases} \mathbf{H}_b^H\mathbf{H}_b & (M_R \ge M_T) \\ \mathbf{H}_b\mathbf{H}_b^H & (M_R < M_T). \end{cases} \quad (6)$$

Here, μ_i is the ith eigenvalue of the Hermitian matrix $\mathbf{Q}$, while assuming continuous-amplitude discrete-time signaling. Moreover, ρ represents the signal-to-noise ratio (SNR). In the CCMC capacity of (5), the employment of ideal ABF weights $\mathbf{F}$ and $\mathbf{W}$ is assumed at the transmitter and the receiver, where $\mathbf{F}$ is the M_T right singular vectors of $\mathbf{H}$ associated with the maximum singular values. Similarly, $\mathbf{W}$ is the M_R left singular vectors of $\mathbf{H}$.

B. DCMC Capacity

Let us now introduce the DCMC capacity C_{DCMC} of mmWave MIMO systems as follows [19], [20]:

$$C_{\mathrm{DCMC}} = B - \frac{1}{2^B}\sum_{f=1}^{2^B} E_{\mathbf{H},\mathbf{n}}\left[\log_2 \sum_{g=1}^{2^B} e^{\eta[f,g]}\right] \text{ [bits/symbol]} \quad (7)$$

where we have

$$\eta[f,g] = \frac{-\|\mathbf{H}_b(\mathbf{x}_f - \mathbf{x}_g) + \mathbf{n}\|^2 + \|\mathbf{n}\|^2}{N_0} \quad (8)$$

and $\mathbf{x}_i$ $(i = 1, \ldots, 2^B)$ represents the legitimate symbol vectors. The ABF weight matrices $\mathbf{F}$ and $\mathbf{W}$ are generated according to the criteria presented in Section III-D. Note that powerful channel coding schemes, such as the turbo codes or low-density parity-check codes, allow us to attain a near-error-free performance close to the DCMC capacity [21].

C. Optimization of ABF-Array Alignment

As previously mentioned, the rank of the MIMO channel matrix in an indoor mmWave scenario is typically low. To circumvent this problem, we optimize the ABF-array alignment according to [9], which increases the rank of the channel matrix. More specifically, to attain the optimum performance in terms of the rank of the channel matrix, the separations of the ABFs D_T and D_R at the transmitter and the receiver have to satisfy the following relationship [9]–[11]:

$$D_T D_R = \frac{\lambda R}{\max(M_T, M_R)\cos(\theta)} \quad (9)$$

where the maximum rank of the channel matrix is given by $\mathrm{rank}(\mathbf{H}_b) = \min(M_T, M_R)$.

D. Criterion for Determining the ABF Weights

If the transmitter knows the accurate estimates of the channel $\mathbf{H}$, which has as many as $(N_T \cdot N_R)$ channel coefficients, it is possible to carry out optimum beamforming at the transmitter and the receiver. However, in practice, it may be a challenging task to acquire all the $(N_T \cdot N_R)$ channel coefficients, particularly for a large-scale MIMO scenario. Hence, in this paper, we control the ABFs based only on the angle-of-departure (AoD) θ_{AoD} and the angle-of-arrival (AoA) θ_{AoA} at the transmitter and the receiver, respectively. This significantly reduces the number of channel coefficients that have to be estimated from the transmitted pilot symbols, namely, from $(N_T \cdot N_R)$ to $(M_T \cdot M_R)$, which is lower than that needed for the full-digital array. More specifically, the ABF weights $\mathbf{f}_i$ and $\mathbf{w}_k$ are given by [10], [13]

$$\mathbf{f}_i = \frac{1}{\sqrt{U_T}}\left[1, \exp\left(j\delta_T^{(i)}\right), \ldots, \exp\left(j(U_T - 1)\delta_T^{(i)}\right)\right]^{\mathrm{T}}$$

$$\mathbf{w}_k = \frac{1}{\sqrt{U_R}}\left[1, \exp\left(j\delta_R^{(k)}\right), \ldots, \exp\left(j(U_R - 1)\delta_R^{(k)}\right)\right]^{\mathrm{T}}$$

TABLE II
SYSTEM PARAMETERS

Fig.	Rate	Scheme	RF	$\mathcal{L}$	Rate	Scheme	RF	$\mathcal{L}$
3	4.0	BF	1	16	8.0	BF	1	256
	4.0	BLAST	2	4	8.0	BLAST	2	16
	4.0	BLAST	4	2	8.0	BLAST	4	4
	4.0	GSM	1	4	8.0	GSM	1	64
	4.0	GSM	2	2	8.0	GSM	2	8
4	8.0	BF	1	256	16.0	BF	1	65536
	8.0	BLAST	2	16	16.0	BLAST	2	256
	8.0	BLAST	8	2	16.0	BLAST	8	4
	8.0	GSM	1	32	17.0	GSM	1	16384
	8.0	GSM	2	4	16.0	GSM	2	64

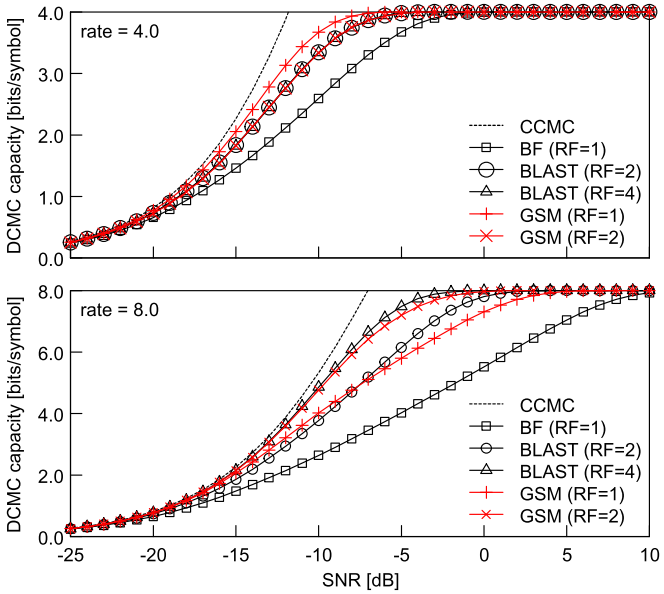

Fig. 3. DCMC capacity comparisons between the GSM and other benchmarks. The transmitter and the receiver had four ABFs, each having four antenna elements and four analog phase shifters. The associated CCMC capacity was also plotted.

where we have $\delta_T^{(i)} = d \cdot (2\pi/\lambda) \cdot \sin(\theta_{\text{AoD}}^{(i)})$ and $\delta_R^{(k)} = d \cdot (2\pi/\lambda) \cdot \sin(\theta_{\text{AoA}}^{(k)})$.[2] Here, $\theta_{\text{AoD}}^{(i)}$ denotes the AoD toward the ith ABF of the receiver, whereas $\theta_{\text{AoA}}^{(k)}$ represents the AoA from the kth ABF of the transmitter.

IV. PERFORMANCE RESULTS

Here, we provide our performance results to characterize the capacity of our GSM scheme, which is compared with the single-stream BF and the spatial-multiplexing benchmark schemes. Throughout the simulations, we assumed the indoor mmWave scenario in Fig. 2, where we have an antenna height of $R = 5$ m. We considered the carrier frequency of 60 GHz, where the corresponding wavelength was $\lambda = 0.5$ cm. The Rice factor K was set to 10.0 dB in accordance with the work in [11]. The antenna spacing d in each ABF was fixed to $\lambda/2$, and the separation between ABFs was optimized based on (9). The employment of omnidirectional antenna elements was assumed both at the transmitter and the receiver. Furthermore, system parameters of all schemes are listed in Table II.

Fig. 3 compares the DCMC capacity of the GSM, the spatial-multiplexing, and the single-stream BF schemes, where the data rates were 4.0 bits/symbol (top) and 8.0 bits/symbol (bottom). The transmitter and the receiver have $N_T = N_R = 16$ antenna elements, which are grouped into $M_T = M_R = 4$ ABFs, where the separation of ABFs was $D_T = D_R = 7.91$ cm. In this scenario, the rank of the channel matrix was $\text{rank}(\mathbf{H}_b) = \min(4, 4) = 4$. For the 4.0-bits/symbol scenario, we considered the 16-QAM single-input single-output (SISO) scheme, the binary phase-shift keying (BPSK)-aided spatial multiplexing having $P = 4$ RF chains, the quaternary phase-shift keying (QPSK)-aided single-RF GSM scheme, and the BPSK-aided GSM having $P = 2$ RF chains. Additionally, the capacity curve of the QPSK-aided spatial-multiplexing scheme using $P = 2$ RF chains was plotted. For the case of 8.0 bits/symbol, the 256-QAM SISO scheme, the QPSK-aided spatial-multiplexing scheme having $P = 4$ RF chains, the 16-QAM-aided spatial-multiplexing scheme using $P = 2$ RF chains, the 64-QAM single-RF GSM scheme, and the 8-PSK GSM scheme having $P = 2$ RF chains were considered. Observe in Fig. 3 that for the rate of 4.0 bits/symbol, the single-RF GSM outperformed the other schemes. Moreover, the DCMC capacity of the GSM having $P = 2$ RF chains was close to those of the spatial-multiplexing schemes that employ $P = 2$ and 4 RF chains. Furthermore, for the rate of 8.0 bits/symbol, the DCMC capacity of the single-RF GSM scheme achieved comparable performance to that of the spatial-multiplexing scheme having $P = 2$ RF chains, whereas the DCMC capacity of the GSM scheme having $P = 2$ RF chains and the spatial-multiplexing scheme having $P = 4$ RF chains exhibited a similar performance at the transmission rate of 4.0 bits/symbol. According to our extensive simulations, it was found that the performance advantage of the proposed scheme remains unchanged in the range of $1 \leq R \leq 5$ m.

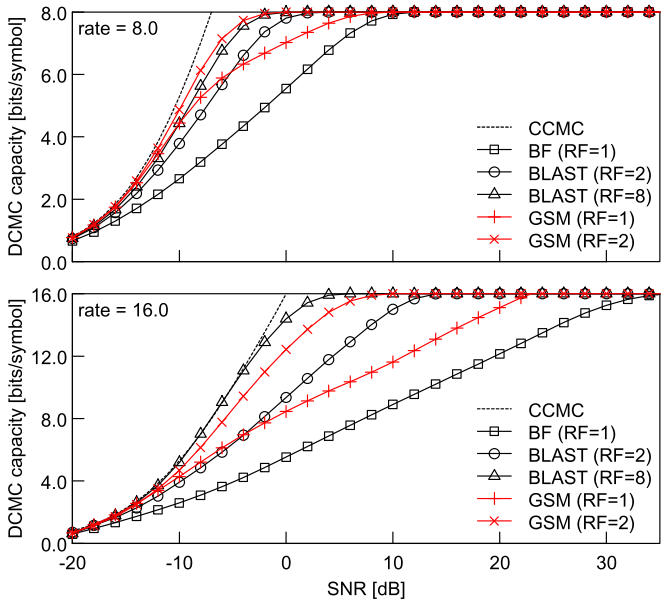

Fig. 4. DCMC capacity comparisons between the GSM and other benchmarks. The transmitter consists of eight ABFs, each having four TA elements, whereas the receiver has four ABFs, each having four receive antenna elements. The associated CCMC capacity was also plotted.

Moreover, Fig. 4 shows the DCMC capacity of the GSM, of the BLAST, and of the SISO schemes for the data rates of 8.0 bits/symbol (top) and 16.0 bits/symbol (bottom). The transmitter and the receiver have $N_T = 32$ and $N_R = 16$ antenna elements, respectively, where the transmitter has $M_T = 8$ ABFs, and the receiver has $M_R = 4$ ABFs. Here, the optimized separation between ABFs was $D_T = D_R = 5.59$ cm. In this scenario, the rank of the channel matrix was $\text{rank}(\mathbf{H}_b) = \min(8, 4) = 4$. For the rate of 8.0 bits/symbol, the 256-QAM SISO scheme, the BPSK-aided spatial-multiplexing scheme

[2]Potentially, the channel state information available at the transmitter allows us to utilize the phase-rotation-based precoding scheme in [22].

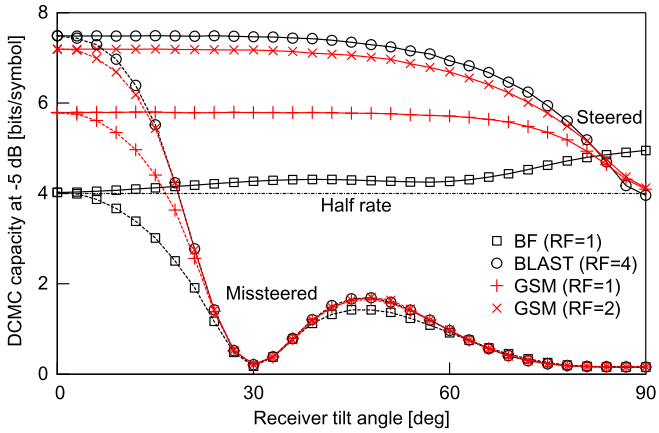

Fig. 5. Effects of the estimated tilt angle $\hat{\theta}$ on the DCMC capacity at the SNR of -5 dB. The system parameters were the same as those used in Fig. 3.

having $P = 8$ RF chains, the 16-QAM spatial-multiplexing scheme using $P = 2$ RF chains, the 32-PSK single-RF GSM scheme, and the QPSK-aided GSM using $P = 2$ RF chains were considered. For the case of 16.0 bits/symbol, the 65536-QAM SISO scheme, the QPSK-aided spatial-multiplexing scheme having $P = 8$ RF chains, the 256-QAM spatial-multiplexing scheme having $P = 2$ RF chains, the 16384-QAM single-RF GSM scheme, and the 64-QAM GSM scheme having $P = 2$ RF chains were compared. For ease of comparison, the data rate of the single-RF GSM was set to 17.0 bits/symbol. It was shown in Fig. 4 that for the rate of 8.0 bits/symbol, the DCMC capacity of the GSM scheme having two RF chains was the highest. For the rate of 16.0 bits/symbol, the full-RF spatial-multiplexing scheme exhibited the best capacity over the entire SNR region, whereas the GSM scheme having two RF chains achieved capacity close to that of the full-RF spatial-multiplexing scheme, where the performance gap was as low as 1.2 dB for the DCMC capacity of 8.0 bits/symbol. Note that the performance advantage of the single-RF GSM scheme was approximately 9.0 dB.

Finally, in Fig. 5, we investigated the effects of the receiver tilt θ, where the system parameters were the same as those used in Fig. 3 (8.0 bits/symbol). The DCMC capacity was calculated at the SNR of -5 dB. We also considered the missteered scenario, where the estimated θ_{AoD} and θ_{AoA} were fixed to 0°. The three capacity curves of the missteered scenario exhibited two peaks, namely, at $\theta = 0^\circ$ and 45°, which corresponded to the directive gains of the main lobe and the sidelobe. When θ_{AoD} and θ_{AoA} were accurately estimated, the capacity of the GSM and of the spatial-multiplexing schemes remained high for the range of $0 \leq \theta < 83^\circ$.

V. Conclusion

In this paper, we have proposed a GSM-based reduced-RF-chain mmWave MIMO system, where the transmitter consists of ABF arrays. In our simulations, we demonstrated that the constrained capacity of our GSM scheme was close to that of its full-RF spatial-multiplexing counterpart, which is equipped with twice or four times higher number of RF chains than the proposed GSM scheme.

References

[1] R. Y. Mesleh, H. Haas, S. Sinanovic, C. Ahn, and S. Yun, "Spatial modulation," *IEEE Trans. Veh. Technol.*, vol. 57, no. 4, pp. 2228–2241, Jul. 2008.

[2] S. Sugiura, C. Xu, S. Ng, and L. Hanzo, "Reduced-complexity coherent versus non-coherent QAM-aided space–time shift keying," *IEEE Trans. Commun.*, vol. 59, no. 11, pp. 3090–3101, Nov. 2011.

[3] C. Xu, S. Sugiura, S. X. Ng, and L. Hanzo, "Spatial modulation and space–time shift keying: Optimal performance at a reduced detection complexity," *IEEE Trans. Commun.*, vol. 61, no. 1, pp. 206–216, Jan. 2013.

[4] M. Di Renzo, H. Haas, A. Ghrayeb, S. Sugiura, and L. Hanzo, "Spatial modulation for generalized MIMO: Challenges, opportunities, and implementation," *Proc. IEEE*, vol. 102, no. 1, pp. 56–103, Jan. 2014.

[5] J. Jeganathan, A. Ghrayeb, and L. Szczecinski, "Generalized space shift keying modulation for MIMO channels," in *Proc. IEEE Int. Symp. PIMRC*, Sep. 2008, pp. 1–5.

[6] S. Sugiura, S. Chen, and L. Hanzo, "Generalized space–time shift keying designed for flexible diversity-, multiplexing- and complexity-tradeoffs," *IEEE Trans. Wireless Commun.*, vol. 10, no. 4, pp. 1144–1153, Apr. 2011.

[7] P. Wolniansky, G. Foschini, G. Golden, and R. Valenzuela, "V-BLAST: An architecture for realizing very high data rates over the rich-scattering wireless channel," in *Proc. ISSSE*, 1998, pp. 295–300.

[8] S. Rangan, T. S. Rappaport, and E. Erkip, "Millimeter-wave cellular wireless networks: Potentials and challenges," *Proc. IEEE*, vol. 102, no. 3, pp. 366–385, Mar. 2014.

[9] F. Bøhagen, P. Orten, and G. E. Øien, "Design of optimal high-rank line-of-sight MIMO channels," *IEEE Trans. Wireless Commun.*, vol. 6, no. 4, pp. 1420–1424, Apr. 2007.

[10] E. Torkildson, U. Madhow, and M. Rodwell, "Indoor millimeter wave MIMO: Feasibility and performance," *IEEE Trans. Wireless Commun.*, vol. 10, no. 12, pp. 4150–4160, Dec. 2011.

[11] L. Zhou and Y. Ohashi, "Fast codebook-based beamforming training for mmWave MIMO systems with subarray structures," in *Proc. IEEE 82nd Veh. Technol. Conf.*, 2015, pp. 1–5.

[12] P. Liu and A. Springer, "Space shift keying for LOS communication at mmWave frequencies," *IEEE Wireless Commun. Lett.*, vol. 4, no. 2, pp. 121–124, Apr. 2015.

[13] Y. J. Guo, X. Huang, and V. Dyadyuk, "A hybrid adaptive antenna array for long-range mm-wave communications," *IEEE Antennas Propag. Mag.*, vol. 54, no. 2, pp. 271–282, Apr. 2012.

[14] O. E. Ayach, S. Rajagopal, S. Abu-Surra, Z. Pi, and R. W. Heath, "Spatially sparse precoding in millimeter wave MIMO systems," *IEEE Trans. Wireless Commun.*, vol. 13, no. 3, pp. 1499–1513, Mar. 2014.

[15] K. Ishibashi and S. Sugiura, "Effects of antenna switching on band-limited spatial modulation," *IEEE Wireless Commun. Lett.*, vol. 3, no. 4, pp. 345–348, Aug. 2014.

[16] I. Sarris and A. R. Nix, "Ricean K-factor measurements in a home and an office environment in the 60 GHz band," in *Proc. 16th IST Mobile Wireless Commun. Summit*, 2007, pp. 1–5.

[17] Y. Shoji, H. Sawada, C. S. Choi, and H. Ogawa, "A modified SV-model suitable for line-of-sight desktop usage of millimeter-wave WPAN systems," *IEEE Trans. Antennas Propag.*, vol. 57, no. 10, pp. 2940–2948, Oct. 2009.

[18] R. Rajashekar, K. V. S. Hari, and L. Hanzo, "Reduced-complexity ML detection and capacity-optimized training for spatial modulation systems," *IEEE Trans. Commun.*, vol. 62, no. 1, pp. 112–125, Jan. 2014.

[19] S. X. Ng and L. Hanzo, "On the MIMO channel capacity of multi-dimensional signal sets," *IEEE Trans. Veh. Technol.*, vol. 55, no. 2, pp. 528–536, Mar. 2006.

[20] S. Sugiura, S. Chen, and L. Hanzo, "Coherent and differential space–time shift keying: A dispersion matrix approach," *IEEE Trans. Commun.*, vol. 58, no. 11, pp. 3219–3230, Nov. 2010.

[21] L. Hanzo, O. Alamri, M. El-Hajjar, and N. Wu, *Near-Capacity Multi-Functional MIMO Systems*. New York, NY, USA: Wiley, 2009.

[22] P. Yang *et al.*, "Phase rotation-based precoding for spatial modulation systems," *IET Commun.*, vol. 9, no. 10, pp. 1315–1323, Jul. 2015.